

Deuterium Kinetic Isotope Effects on the Dissociation of a Protein–Fatty Acid Complex in the Gas Phase

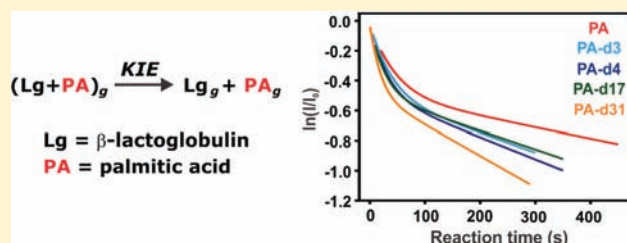
Lan Liu,^{†,‡} Klaus Michelsen,[§] Elena N. Kitova,^{†,‡} Paul D. Schnier,[§] Alex Brown,[†] and John S. Klassen^{*,†,‡}

[†]Department of Chemistry and [‡]Alberta Glycomics Centre, University of Alberta, Edmonton, Alberta, Canada T6G 2G2

[§]Molecular Structure, Amgen, Thousand Oaks, California 91320, United States

S Supporting Information

ABSTRACT: Deuterium kinetic isotope effects (KIEs) are reported for the first time for the dissociation of a protein–ligand complex in the gas phase. Temperature-dependent rate constants were measured for the loss of neutral ligand from the deprotonated ions of the 1:1 complex of bovine β -lactoglobulin (Lg) and palmitic acid (PA), $(\text{Lg} + \text{PA})^{n-} \rightarrow \text{Lg}^{n-} + \text{PA}$, at the 6– and 7– charge states. At 25 °C, partial or complete deuteration of the acyl chain of PA results in a measurable inverse KIE for both charge states. The magnitude of the KIEs is temperature dependent, and Arrhenius analysis of the rate constants reveals that deuteration of PA results in a decrease in activation energy. In contrast, there is no measurable deuterium KIE for the dissociation of the (Lg + PA) complex in aqueous solution at pH 8. Deuterium KIEs were calculated using conventional transition-state theory with an assumption of a late dissociative transition state (TS), in which the ligand is free of the binding pocket. The vibrational frequencies of deuterated and non-deuterated PA in the gas phase and in various solvents (*n*-hexane, 1-chlorohexane, acetone, and water) were established computationally. The KIEs calculated from the corresponding differences in zero-point energies account qualitatively for the observation of an inverse KIE but do not account for the magnitude of the KIEs nor their temperature dependence. It is proposed that the dissociation of the (Lg + PA) complex in aqueous solution also proceeds through a late TS in which the acyl chain is extensively hydrated such that there is no significant differential change in the vibrational frequencies along the reaction coordinate and, consequently, no significant KIE.



INTRODUCTION

The association and dissociation of noncovalent protein–ligand interactions are critical events in many biological processes, such as transport, signaling, chemical transformation, and molecular and cellular recognition.^{1–4} Knowledge of the forces that control the rates of these processes and the underlying reaction mechanisms is of fundamental importance and facilitates the design of novel therapeutics. The rates of protein–ligand association reactions are often dominated by the diffusion properties of the ligand,⁵ although other factors such as electrostatic effects and binding site accessibility may also play a role.^{5–7} In contrast, the details of the dissociation reactions are poorly understood.⁸ The rate of ligand escape from the binding pocket of a protein may be strongly affected by many factors, such as the number and nature of the intermolecular interactions that must be broken in order for the ligand to be released from the pocket, protein structural changes that accompany ligand release, and reorganization of solvent molecules during the dissociation process.^{5,9}

Given the inherently intricate nature of the dissociation process, developing a detailed, quantitative understanding of how a ligand escapes from the binding pocket represents a significant challenge.¹⁰ One promising approach to this problem is based on the dissociation kinetics of protein–ligand complexes measured in their desolvated state (i.e., in the gas

phase). The advantage of a “gas-phase” approach is that it affords an opportunity to probe the kinetics and mechanisms of dissociation reactions free from the complicating effects of solvent.^{11,12} Furthermore, comparison of the gas-phase data with kinetic data measured in solution can, in principle, provide quantitative insights into the role of solvent in the dissociation reactions.^{11–13}

Recently, the dissociation reactions of bovine β -lactoglobulin (Lg) complexed with a series of long-chain fatty acids (FAs) were investigated in the gas phase.¹⁴ Lg, an 18 kDa whey protein, possesses a large and flexible cavity that can accommodate a variety of hydrophobic ligands, including FAs such as palmitic acid (PA).^{15,16} According to the crystal structure of the (Lg + PA) complex (PDB 1B0O), the acyl chain of PA is fully buried within the hydrophobic cavity, while the carboxyl group is located near the top of the cavity and is exposed to solvent. It was shown using electrospray ionization mass spectrometry (ESI-MS) that the interaction between Lg and PA, and other long chain FAs, can be transferred, intact, from aqueous solution to the gas phase.¹⁴ Notably, gaseous deprotonated $(\text{Lg} + \text{FA})^{n-}$ ions, where $n = 6$ and 7, adopt one of two non-interconverting structures, which are referred to as

Received: January 4, 2012

Published: March 12, 2012

the fast and slow dissociating components, $(\text{Lg} + \text{PA})_f^{n-}$ and $(\text{Lg} + \text{PA})_s^{n-}$, respectively. The kinetic data measured for the loss of neutral FA from $(\text{Lg} + \text{FA})^{n-}$ ions, together with the results of molecular dynamics (MD) simulations, suggest that the acyl chain of the FAs is retained within the hydrophobic cavity of Lg in the gas phase, at least for the fast components.¹³ In the $(\text{Lg} + \text{PA})_f^{n-}$ ions, PA is believed to be stabilized predominantly by protein–lipid interactions, while for the $(\text{Lg} + \text{PA})_s^{n-}$ ions, H-bonds between the ligand carboxyl group and Lg are also thought to contribute to the stability of the complex.¹⁴ Interestingly, comparison of the dissociation rate constants measured for gaseous deprotonated $(\text{Lg} + \text{FA})^{n-}$ ions with those determined in aqueous solution (at pH 8) revealed that the hydrated $(\text{Lg} + \text{FA})$ complexes are kinetically less stable at room temperature. The lower kinetic stability of the hydrated $(\text{Lg} + \text{FA})$ complexes results from a lower dissociation activation energy (E_a).¹³ Importantly, the differences in E_a values measured in the gas phase and in water are consistent with the enthalpy changes expected for the hydration of the acyl chain of the FAs. These results led to the hypothesis that dissociation of the $(\text{Lg} + \text{FA})$ complexes, both in aqueous solution and in the gas phase, proceeds through a late transition state (TS), in which the ligand has almost fully escaped the binding pocket.¹³

Here, deuterium kinetic isotope effects (KIEs) were exploited to further investigate the dissociation mechanism of the $(\text{Lg} + \text{PA})$ complex in aqueous solution and in the gas phase. A deuterium KIE corresponds to the ratio of the rate constants for the non-deuterated and deuterated reactants, i.e., k_H/k_D . Deuterium KIEs typically arise from changes in the vibrational frequencies of the bonds involving the isotopes in the reactant form (R) and the TS. These changes, which differ for the non-deuterated and deuterated forms of the reactant, affect the change in zero-point energy (ΔZPE) and, correspondingly, the E_a of the reaction.¹⁷ The magnitude of the KIE resulting from the differential change in ΔZPE can be estimated using transition-state theory:

$$\text{KIE} \approx e^{-\Delta\Delta\text{ZPE}/RT} \quad (1)$$

where $\Delta\Delta\text{ZPE}$ is the difference in ΔZPE corresponding to reactions involving the non-deuterated and deuterated reactants ($\Delta\Delta\text{ZPE} = \Delta\text{ZPE}_H - \Delta\text{ZPE}_D$). Deuterium KIEs for unimolecular reactions are also sensitive to differential changes in the rotational and vibrational partition functions of the non-deuterated and deuterated reactants on going from R to the TS. However, the influence of changes in the rotational and vibrational partition functions on the rate constant is usually small compared to those resulting from changes in ΔZPE .¹⁷

Deuterium KIEs can serve as a sensitive probe of reaction mechanisms and have been used extensively to characterize a variety of chemical and biochemical reactions in solution.^{18–22} Deuterium KIEs have also been used to probe mechanisms of reactions occurring in the gas phase.^{11,12,23–27} However, to our knowledge, no quantitative studies of deuterium KIEs for the dissociation of biological complexes in the gas phase have been previously reported. In the present study, rate constants for the dissociation of deprotonated $(\text{Lg} + \text{PA})_f^{7-}$ and $(\text{Lg} + \text{PA})_s^{6-}$ ions composed of partially and fully deuterated PA— $\text{CD}_3(\text{CH}_2)_{14}\text{COOH}$ (D3), $\text{CH}_3(\text{CH}_2)_7(\text{CD}_2)_2(\text{CH}_2)_5\text{COOH}$ (D4), $\text{CD}_3(\text{CD}_2)_7(\text{CH}_2)_7\text{COOH}$ (D17), and $\text{CD}_3(\text{CD}_2)_{14}\text{COOH}$ (D31)—were measured using the black-body infrared radiative dissociation (BIRD) technique^{28,29} and Fourier-transform ion cyclotron resonance (FTICR) MS.

These kinetic data were then compared to those reported recently for non-deuterated PA (D0) with the goal of probing the structure of the dissociative TS.¹³ The effects of deuteration and solvation on the vibrational frequencies of PA were investigated computationally to assist in the interpretation of the observed KIEs. Rate constants were also measured for the dissociation of the $(\text{Lg} + \text{PA})$ complex, composed of PA (D31), in aqueous solution at pH 8 and temperatures ranging from 5 to 32 °C using surface plasmon resonance (SPR) spectroscopy. These data were then compared to results reported for the $(\text{Lg} + \text{PA})$ complex composed of PA (D0) to evaluate the influence of solvent on the KIEs.¹³

EXPERIMENTAL SECTION

Sample Preparation. Bovine β -lactoglobulin (Lg, monomer average MW 18 281 Da), palmitic acid (PA, 256 Da), and PA-d31 (D31, 287 Da) were purchased from Sigma-Aldrich Canada (Oakville, Canada). Palmitic acid-methyl- d_3 (D3, 259 Da), PA-7,7,8,8-D4 (D4, 260 Da), and PA-9,9...16,16,16-D17 (D17, 273 Da) were purchased from ACP Chemicals (St. Leonard, Canada). The Lg was dissolved and exchanged directly into Milli-Q water using an Amicon microconcentrator with a molecular weight cutoff of 10 kDa. The concentration of the Lg solution was determined by lyophilizing a known volume of the filtrate and measuring the mass of the protein. The protein stock solution was stored at -20 °C. The ligand stock solutions were prepared by dissolving PA into aqueous ammonium acetate. The ESI solutions were prepared from stock solutions of protein and ligand; imidazole (10 mM) was also added in order to stabilize the $(\text{Lg} + \text{PA})$ complexes during ESI-MS analysis. Aqueous ammonium hydroxide was added to adjust the pH of the solution to 8.5.

Mass Spectrometry. Experimental measurements were performed using an Apex II 9.4 T Fourier-transform ion cyclotron resonance (FTICR) mass spectrometer (Bruker, Billerica, MA) equipped with a modified external nanoflowES (nanoESI) ion source. NanoESI was performed using borosilicate tubes (1.0 mm o.d., 0.68 mm i.d.), pulled to ~ 5 μm o.d. at one end using a P-2000 micropipet puller (Sutter Instruments, Novato, CA). The electric field required to spray the solution in negative-ion mode was established by applying a voltage of ~ -800 V to a platinum wire inserted inside the glass tip. The solution flow rate was typically ~ 20 nL min^{-1} . The gaseous ions produced by nanoESI were introduced into the mass spectrometer through a stainless steel capillary (i.d. 0.43 mm) maintained at an external temperature of 66 °C. The gas flow rate into the instrument was measured to be 0.6 L min^{-1} . The ions sampled by the capillary (-50 V) were transmitted through a skimmer (0 V) and accumulated electrostatically in an rf hexapole. Ions were then ejected from the hexapole and accelerated ($+2700$ V) into the superconducting magnet, decelerated, and introduced into the ion cell. The trapping plates of the cell were maintained at a constant potential of -1.4 V throughout the experiment. Two flexible heating blankets placed around the portion of the vacuum tube that surrounds the ion cell were used to control the temperature of the ion cell for the BIRD experiments. The typical base pressure for the instrument was $\sim 5 \times 10^{-10}$ mbar. Data acquisition was controlled by an SGI R5000 computer running the Bruker Daltonics XMASS software, version 5.0. Mass spectra were obtained using standard experimental sequences with chirp broadband excitation. The time domain signal, consisting of the sum of 50 transients containing 128K data points per transient, was subjected to one zero-fill prior to Fourier transformation.

Analysis of Kinetic Data. As described above, the deprotonated $(\text{Lg} + \text{PA})^{n-}$ ions, where $n = 6$ or 7 , exist in two kinetically distinct structures, designated as the $(\text{Lg} + \text{PA})_f^{n-}$ and $(\text{Lg} + \text{PA})_s^{n-}$ ions. At the temperatures investigated, both structures dissociate exclusively by the loss of neutral PA with dissociation rate constants, k_f and k_s , respectively:



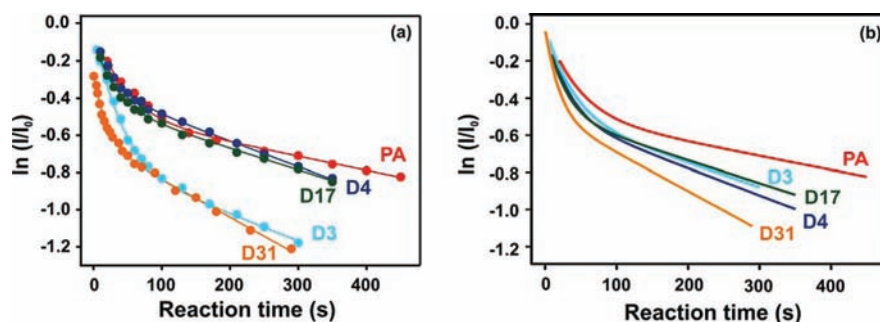


Figure 1. (a) Plots of the natural logarithm of the normalized intensity (I/I_0) of $(\text{Lg} + \text{PA})^{7-}$ ions versus reaction time measured at 25 °C for PA = D0 (red), D3 (blue), D4 (black), D17 (green), and D31 (orange). The solid curves correspond to the best fits of double exponential decay functions to the experimental data. (b) Simulated kinetic plots calculated from the rate constants determined from plots in (a) and using a constant fraction of fast and slow components, 0.37 and 0.63, respectively.



The dissociation rate constants and abundance of the individual components were determined by fitting a double exponential function to the time-dependent normalized intensities (I/I_0) of the $(\text{Lg} + \text{PA})^{n-}$ ions:

$$I/I_0 = X_{f,0} e^{-k_f t} + X_{s,0} e^{-k_s t} \quad (3)$$

where $X_{f,0}$ and $X_{s,0}$ correspond to the initial fractions of the fast and slow components, respectively. At a given reaction time, the normalized intensity of the reactant ion was calculated using eq 4:

$$I/I_0 = I_{(\text{Lg}+\text{PA})} / (I_{(\text{Lg}+\text{PA})} + I_{\text{Lg}}) \quad (4)$$

where $I_{(\text{Lg}+\text{PA})}$ and I_{Lg} are the measured intensities of the corresponding $(\text{Lg} + \text{PA})^{n-}$ and Lg^{n-} ions, respectively. To improve the accuracy of the curve fitting, $X_{s,0}$ and k_s were first estimated by fitting the kinetic data obtained at long reaction times, which reflect only the slow component, with a single exponential function. Incorporating the k_s and $X_{s,0}$ values into eq 3 and fitting this to the I/I_0 versus reaction time data allowed k_f and $X_{f,0}$ to be determined.

Surface Plasmon Resonance Spectroscopy. Surface plasmon resonance (SPR) spectroscopy measurements were performed on a Biacore T100 instrument (GE Healthcare). Reagents used were obtained from Sigma-Aldrich, Isotec, or GE Healthcare. Immobilization running buffer consisted of 10 mM Hepes pH 7.4, 150 mM NaCl, and 0.2 mM TCEP. Lg was immobilized onto a carboxymethyl dextran (CMS) chip using amine coupling chemistry at 25 °C. Surfaces were first pre-conditioned with two 6 s pulses each of 100 mM HCl, 50 mM NaOH, and 0.5% (w/v) SDS at a flow rate of 100 $\mu\text{L min}^{-1}$. At a flow rate of 10 $\mu\text{L min}^{-1}$, CMS surface was activated for 7 min with a mixture of NHS/EDC, followed by a 90 s injection of 20 $\mu\text{g mL}^{-1}$ Lg in 10 mM sodium acetate pH 4.0. Remaining activated groups were subsequently blocked with a 7 min injection of ethanolamine. Using this approach, 600 RU of Lg was immobilized. Kinetic measurements were conducted in buffer consisting of 25 mM Tris pH 8.0, 1 mM TCEP, 0.2 mM CHAPS, and 8% (v/v) methanol. Stock solutions of PA and PA(D31) were prepared in methanol, and serial dilutions of the FAs were performed in methanol. Diluted FAs were subsequently added to the buffer to a final methanol concentration of 8% (v/v) methanol. The FAs were injected over the Lg surface for 30 s association and dissociation monitored for 60 s at a flow rate of 80 $\mu\text{L min}^{-1}$. The sample analysis temperature was varied between 5 and 32 °C.

Data were processed using the Biacore T100 analysis software and Igor Pro (Wavemetrics Inc.). Sensorgrams were corrected for systematic noise and baseline drift by subtracting the response of the reference spot, which was activated but not exposed to protein. The average response from blank injections was used to double-reference the binding data. The dissociation portion of the sensorgrams were de-spiked, binomial smoothed, and fitted to an exponential function to determine the dissociation rate constants.

Computational Methods. Geometries of PA were optimized using Becke's three-parameter hybrid functional (B3LYP)^{30–33} and the hybrid Perdew, Burke, and Ernzerhof functional (PBE0),^{34–36} both with the standard 6-311+G(d,p) basis set for all atoms.³⁷ Geometry optimizations were performed in the gas phase and in solvents (*n*-hexane, 1-chlorohexane, acetone, and water) using the IEF-PCM polarizable continuum model,^{38–40} as implemented in Gaussian09.⁴¹ The dielectric constants for the solvents *n*-hexane, 1-chlorohexane, acetone, and water are 1.88, 5.95, 20.49, and 78.36, respectively. All geometry optimizations used tight convergence thresholds as defined by maximum force equal to 1.5×10^{-5} a.u., rms force of 1.0×10^{-5} a.u., maximum displacement of 6.0×10^{-5} a.u., and rms displacement of 4.0×10^{-5} a.u. In all cases, the optimized geometry was that of the fully extended PA chain, although all calculations were carried out with C_1 symmetry. From the X-ray crystal structure of the $(\text{Lg} + \text{PA})$ complex (PDB 1B00), the chain is not fully extended due to the specific interactions within the protein cavity. However, the use of the fully extended geometry is satisfactory for the static structure and continuum models considered here. In the vibrational analysis, corrections for hindered and free internal rotations^{42–44} were made in order to assess the influence of neglect/inclusion of these effects on the ZPE.

RESULTS AND DISCUSSION

Deuterium Kinetic Isotope Effects in the Gas Phase. At reaction temperatures of 25–66 °C, BIRD of the $(\text{Lg} + \text{PA})^{7-}$ ions results exclusively in the loss of neutral PA. Shown in Figure S1 (Supporting Information) are natural log plots of the normalized intensities of the reactant ions versus time measured for the $(\text{Lg} + \text{PA})^{7-}$ ions composed of non-deuterated (D0) and deuterated forms of PA (D3, D4, D17, and D31) at several temperatures. Notably, each of the kinetic plots exhibits non-linear behavior, which can be described by double exponential functions, consistent with the presence of two distinct structures. Shown together in Figure 1a are the kinetic data for each of the $(\text{Lg} + \text{PA})^{7-}$ ions measured at 25 °C. Because the relative abundance of the $(\text{Lg} + \text{PA})_f^{7-}$ and $(\text{Lg} + \text{PA})_s^{7-}$ ions tends to vary between experiments (presumably due to differences in the ESI droplet histories), it is difficult to establish the influence of deuteration on the kinetic stability directly from visual inspection of the kinetic plots. Shown in Figure 1b are synthesized kinetic plots constructed from the rate constants measured from the data shown in Figure 1a for the $(\text{Lg} + \text{PA})_f^{7-}$ and $(\text{Lg} + \text{PA})_s^{7-}$ ions (k_f and k_s , respectively) and using constant fractions for the $(\text{Lg} + \text{PA})_f^{7-}$ and $(\text{Lg} + \text{PA})_s^{7-}$ ions ($X_{f,0} = 0.37$ and $X_{s,0} = 0.63$, respectively). It can be seen that, at 25 °C, deuteration of PA results in larger rate constants for both the fast and slow components. The deuterium KIEs range from 0.82 ± 0.10 (D3)

to 0.42 ± 0.09 (D31) for the fast component and from 0.57 ± 0.10 (D3) to 0.36 ± 0.04 (D31) for the slow component (Table 1). Deuterium KIEs were also determined for the (Lg +

Table 1. Rate Constants (k) and Kinetic Isotope Effects (KIE) Measured at 25 and 51 °C for Dissociation of the Gaseous Deprotonated (Lg + PA)_f⁷⁻ and (Lg + PA)_s⁷⁻ Ions Composed of Non-deuterated (D0) and Deuterated PA (D3, D4, D17, and D31)^a

T (°C)	PA	k (s ⁻¹)	KIE		
25	D0	Fast			
		0.026 ± 0.0013			
		D3	0.031 ± 0.00323	0.82 ± 0.10	
		D4	0.038 ± 0.004	0.68 ± 0.08	
		D17	0.043 ± 0.0046	0.60 ± 0.03	
	D31	0.060 ± 0.0130	0.42 ± 0.09		
	D0	Slow			
		0.00076 ± 0.000081			
		D3	0.0013 ± 0.00018	0.57 ± 0.10	
		D4	0.0014 ± 0.000049	0.55 ± 0.06	
		D17	0.0012 ± 0.000073	0.60 ± 0.07	
		D31	0.0021 ± 0.00013	0.36 ± 0.04	
		51	D0	Fast	
				0.22 ± 0.016	
				D3	0.25 ± 0.020
D4				0.29 ± 0.014	0.75 ± 0.07
D17	0.23 ± 0.017			0.96 ± 0.10	
D31	0.36 ± 0.032		0.61 ± 0.07		
D0	Slow				
	0.016 ± 0.0010				
	D3		0.026 ± 0.0034	0.63 ± 0.09	
	D4		0.022 ± 0.0012	0.74 ± 0.06	
	D17	0.017 ± 0.0016	0.96 ± 0.11		
D31	0.018 ± 0.0014	0.89 ± 0.09			

^aErrors correspond to one standard deviation.

PA)⁷⁻ ions at 51 °C (Table 1) and the corresponding (Lg + PA)⁶⁻ ions at 25 and 51 °C (Table S1). Notably, the KIEs measured for the dissociation of the (Lg + PA)⁶⁻ ions are consistent in magnitude with those observed for the (Lg + PA)⁷⁻ ions.

Shown in Figure S2 are Arrhenius plots for the dissociation of the (Lg + PA)_f⁷⁻ and (Lg + PA)_s⁷⁻ ions for deuterated and non-deuterated PA. Inspection of the Arrhenius parameters (E_a , A) reveals that deuteration results in a decrease in E_a , although the magnitude of the effect does not scale linearly with deuterium incorporation (Table 2). For the fast components, the decrease in E_a ranges from 1 to 3 kcal mol⁻¹, while for the slow components the effect is more significant, 2–7 kcal mol⁻¹. Because deuteration results in a change in E_a , as well as A , the magnitude of the KIE is temperature dependent. As a result, inverse KIEs (<1) observed near room temperature will eventually become normal KIEs (>1) at higher temperatures. For this reason it is, perhaps, more convenient to describe the effect of deuteration on the dissociation kinetics in terms of the change in E_a , i.e., the activation energy isotope effect, ΔE_a IE (Table 2).

To establish whether the incorporation of deuterium into Lg also influences the rate of ligand loss from the (Lg + PA)ⁿ⁻ ions, kinetic measurements were performed on deuterated (Lg + PA)⁷⁻ ions, i.e., (D-Lg + PA)⁷⁻ ions, produced from D₂O. Shown in Figure S3 is a representative ESI mass spectrum

Table 2. Arrhenius Parameters (E_a , A) and Corresponding ΔE_a IE Values Determined for the Dissociation of the Gaseous Deprotonated (Lg + PA)_f⁷⁻ and (Lg + PA)_s⁷⁻ Ions for Non-deuterated PA (D0) and Deuterated PA (D3, D4, D17, and D31)^a

PA	E_a (kcal mol ⁻¹)	ΔE_a IE ^b (kcal mol ⁻¹)	A (s ⁻¹)
Fast			
D0	16.2 ± 0.2	–	$10^{10.3 \pm 0.1}$
D3	15.4 ± 0.2	0.8 ± 0.3	$10^{9.8 \pm 0.2}$
D4	15.1 ± 0.2	1.1 ± 0.3	$10^{9.7 \pm 0.1}$
D17	13.8 ± 0.5	2.4 ± 0.5	$10^{8.7 \pm 0.4}$
D31	12.9 ± 0.2	3.3 ± 0.3	$10^{8.2 \pm 0.2}$
Slow			
D0	23.6 ± 0.6	–	$10^{14.2 \pm 0.4}$
D3	21.1 ± 0.4	2.5 ± 0.7	$10^{12.6 \pm 0.3}$
D4	19.9 ± 0.3	3.7 ± 0.7	$10^{11.8 \pm 0.2}$
D17	19.3 ± 0.2	4.3 ± 0.6	$10^{11.3 \pm 0.1}$
D31	16.8 ± 0.5	6.8 ± 0.9	$10^{9.6 \pm 0.3}$

^aThe reported errors are one standard deviation. ^b ΔE_a IE = $E_{a,D0} - E_{a,Dx}$ where $x = 3, 4, 17, \text{ or } 31$.

obtained following incubation of Lg in D₂O for 30 min at 25 °C. Analysis of the mass spectrum reveals an average increase of ~80 Da in the MW of Lg. Because water is excluded from the cavity of Lg, even in the absence of ligand binding,⁴⁵ the residues in the cavity are expected to undergo little or no exchange. Plotted in Figure S4 are the kinetic data measured for the (Lg + PA)⁷⁻ and (D-Lg + PA)⁷⁻ ions at 66 °C. Comparison of these kinetic data with those measured for non-deuterated (Lg + PA)⁷⁻ ions, under identical conditions, fails to reveal a KIE. These results indicate that the incorporation of deuterium remote from the binding cavity does not produce a KIE. These results also serve to exclude the possibility that the KIEs measured for the (Lg + PA)ⁿ⁻ ions consisting of deuterated PA reflect subtle differences in the temperature of the deuterated and non-deuterated ions due to differences in radiative energy transfer or any mass discrimination effects resulting from differential trapping of the deuterated and non-deuterated (Lg + PA)ⁿ⁻ ions.

Origin of Deuterium KIEs in Gas Phase. There is abundant evidence for equilibrium deuterium isotope effects on non-covalent interactions involving nonpolar or weakly polar molecules. For example, Shi and Davis reported on the gas chromatographic separation of pairs of deuterated and non-deuterated molecules using squalane and silicone oil columns.⁴⁶ For each pair of compounds they observed an inverse isotope effect with the deuterated analogues eluting first. Their results were interpreted in terms of a differential decrease in the C–H/C–D vibrational modes, and correspondingly the ZPEs, of the compounds due to van der Waals interactions with the condensed phase. Several laboratories have employed reversed-phase liquid chromatography to investigate deuterium isotope effects on hydrophobic bonding.^{17,47,48} These studies have consistently shown that, in the presence of a polar mobile phase, deuterated compounds are less well retained than their non-deuterated counterparts. Solvent-induced changes in the vibrational frequencies of C–H/C–D bonds, in particular the high-frequency stretching modes, have been suggested as the origin of these isotope effects.^{47,48}

The observation of inverse of the KIEs for the dissociation of the gaseous (Lg + PA)ⁿ⁻ ions are qualitatively consistent with differential changes in the vibrational frequencies of non-

Table 3. Vibrational Zero-Point Energies of PA (D0), Partially Deuterated PA (D3), and Deuterated PA (D31) As Determined at the B3LYP/6-311+G(d,p) and PBE0/6-311+G(d,p) Levels of Theory^a

solvent	ZPE for D0 (Δ ZPE)	ZPE for D3 (Δ ZPE)	$\Delta\Delta$ ZPE for D3	ZPE for D31 (Δ ZPE)	$\Delta\Delta$ ZPE for D31
B3LYP/6-311+G(d,p)					
gas phase	287.461	281.451	–	223.236	–
<i>n</i> -hexane	287.217 (0.244)	281.214 (0.237)	0.007	223.042 (0.194)	0.050
1-chlorohexane	286.917 (0.544)	280.924 (0.527)	0.017	222.804 (0.432)	0.112
acetone	286.774 (0.687)	280.785 (0.666)	0.021	222.692 (0.544)	0.143
water	286.723 (0.738)	280.735 (0.716)	0.027	222.651 (0.585)	0.153
PBE0/6-311+G(d,p)					
gas phase	289.140	283.107	–	224.749	–
<i>n</i> -hexane	288.903 (0.237)	282.877 (0.230)	0.007	224.561 (0.188)	0.049
1-chlorohexane	288.583 (0.557)	282.567 (0.540)	0.017	224.307 (0.442)	0.115
acetone	288.420 (0.720)	282.409 (0.698)	0.022	224.179 (0.570)	0.150
water	288.361 (0.779)	282.351 (0.756)	0.023	224.133 (0.616)	0.163

^a. Energies are in kcal mol⁻¹. The differences between the gas-phase and solvent-phase ZPE values, Δ ZPE = ZPE_{gas phase} – ZPE_{solvent}, are given, as are the corresponding $\Delta\Delta$ ZPE.

deuterated and deuterated complex along the reaction coordinate (i.e., in going from R to the TS). In the bound form, the acyl chain of PA is solvated by the hydrophobic residues that line the binding pocket of Lg. The major interactions are expected to involve dipole–induced dipole and London dispersion forces. In the dissociative TS, the acyl chain will necessarily be solvated less by Lg. As discussed elsewhere, the C–H stretching modes of alkanes exhibit solvent-induced frequency shifts of several cm⁻¹; generally, the frequencies are lower in solution than in the gas phase.^{48,49} As a result, a net increase in the magnitude of the acyl chain C–H vibrational frequencies is expected to occur along the reaction coordinate. An increase in the vibrational frequencies will lead to an increase in the TS vibrational ZPE, compared to that of R. Because of the larger mass of D, compared to H, the amplitude of vibrations, as well as polarizabilities and average volumes, of C–D bonds are smaller than those of the corresponding C–H bonds.¹⁷ Due to the lower bond polarizabilities and smaller average volumes of the C–D bonds, the interactions between Lg and deuterated PA are expected to be weaker than those involving PA. Therefore, the influence of protein solvation on the vibrational frequencies associated with the acyl chain will be greater for PA (D0), compared to the deuterated analogues. Consequently, desolvating the acyl chain along the reaction coordinate will influence differently the Δ ZPEs for the deuterated and non-deuterated PA.

To assess whether differential changes in the vibrational frequencies of PA, alone, during dissociation can account for the magnitude of the inverse deuterium KIEs, the vibrational frequencies of fully deuterated (D31), partially deuterated (D3), and non-deuterated PA (D0) and the influence of solvent thereon, were investigated computationally. The PCM approach, which gives reasonable predictions of the change in vibrational frequency upon solvation,^{50,51} was used to approximate the dielectric properties of the Lg cavity (the “solvent”), while neglecting any specific solute–“solvent” interactions. The ZPEs of PA (D0), PA (D3), and PA (D31) in the gas phase and in solvent were determined at the B3LYP/6-311+G(d,p) and PBE0/6-311+G(d,p) levels of theory (Table 3). From these results, the change in ZPE (i.e., Δ ZPE) in going from the solvent, which is taken to approximate R, to the gas phase, which approximates the late TS, was determined. From these values, the difference in Δ ZPE (i.e., $\Delta\Delta$ ZPE) was calculated. As seen in Table 3, the effects are very small

(ranging from ~0.01 to 0.02 kcal mol⁻¹ for D3 and from ~0.1 to 0.2 kcal mol⁻¹ for D31) and increase going from *n*-hexane to water, i.e., with increasing dielectric constant. The ZPEs can be corrected using known gas-phase scaling factors,⁵² but while scaling changes the magnitude of the Δ ZPE values, it does not significantly impact the magnitude of the $\Delta\Delta$ ZPE values (Table S2). One can also consider the change in internal energies (ΔE_{int}), at 25 °C, in going from R to TS, and, more importantly, the effects of isotopic substitution on this change ($\Delta\Delta E_{\text{int}}$). As seen in Table S3, the $\Delta\Delta E_{\text{int}}$ are similar in magnitude to the calculated $\Delta\Delta$ ZPE values. Incorporation of frequency scaling (Table S4) or accounting for hindered rotations (Table S5) results in a small increase in the $\Delta\Delta E_{\text{int}}$ values, up to 0.3 kcal mol⁻¹.

Analysis of the vibrational frequencies calculated for PA (D0), PA (D3), and PA (D31) in the gas phase and using the IEF-PCM polarizable continuum model reveals small positive $\Delta\Delta$ ZPEs, which would result in an inverse KIE. However, the magnitudes of the calculated $\Delta\Delta$ ZPE values do not account quantitatively for the observed KIEs and systematically underestimate the ΔE_a IE values. For example, at 25 °C, a $\Delta\Delta$ ZPE of 0.2 kcal mol⁻¹ corresponds to a KIE of 0.71, which is approximately 2 times “smaller” than the experimentally determined KIEs for PA (D31), 0.42 (fast), and 0.36 (slow). The discrepancies between the experimental and calculated KIEs and ΔE_a IEs can reasonably be attributed to the neglect of the protein structure and the specific intermolecular interactions (which are expected to be dominated by dipole–induced dipole and dispersion forces) that stabilize the complex, in the analysis. The increased conformational flexibility of the acyl chain in the TS may also contribute to the experimental KIEs and ΔE_a IEs. In an effort to better understand why the IEF-PCM approach underestimates the magnitude of the measured KIEs, our laboratory is currently applying DFT methods that take into account dispersion forces to evaluate interactions between PA and the amino acids that are located in the binding cavity of Lg.

The theoretical treatment of the vibrational frequencies of PA (D0), PA (D3), and PA (D31) in the gas phase and using the IEF-PCM polarizable continuum model, together with transition state theory, does not account quantitatively for the observed KIEs, nor the ΔE_a IE values. However, the results of this analysis do suggest that a reduction in the intermolecular Lg–lipid interactions along the reaction coordinate leads to a

differential change in the vibrational frequencies of the deuterated and non-deuterated complexes and give rise to an inverse KIE. It follows that the measurable KIE found for PA (D3), in which only the methyl group is deuterated, together with computational evidence of the collapse of the Lg cavity upon removal of PA in the gas phase,¹⁴ is consistent with a late dissociative TS, wherein the acyl chain is free of the cavity or nearly so. It should be noted that this hypothesis is also supported by the similarity in the E_a values determined for the gaseous deprotonated (Lg + FA)⁷⁻ ions composed of FAs with different chain lengths and the enthalpies estimated for the solvation of the acyl chain of the FAs by nonpolar or weakly polar organic solvents.¹⁴

Absence of Deuterium KIEs in Solution. To our knowledge, deuterium KIEs have not been previously reported for the dissociation of protein–ligand complexes in solution. Therefore, it was also of interest to test whether KIEs could be detected for the dissociation of the (Lg + PA) complex in aqueous solution. Dissociation rate constants were measured for the (Lg + PA) complex, composed of PA (D31) at pH 8 and temperatures ranging from 5 to 32 °C, using SPR spectroscopy, and these results were compared to kinetic data reported previously for PA (D0). Plotted in Figure 2 are the

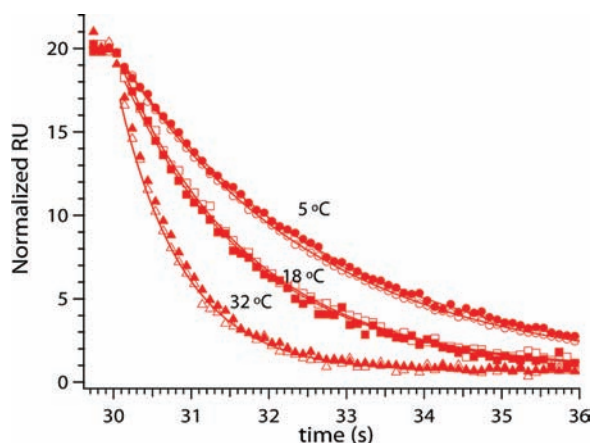


Figure 2. SPR kinetic plots and exponential fits for (Lg + PA) (filled symbols) and (Lg + D31) (open symbols) at the temperatures indicated.

dissociation portions of SPR sensorgrams for the (Lg + PA) complex composed of PA (D31) and PA (D0) versus time at the temperatures indicated. Interestingly, there is no measurable KIE at any of the temperatures investigated. Based on the aforementioned arguments, these observations, on their own, could be viewed as evidence of an early dissociative TS, in which there is little change in the extent to which the ligand is solvated by Lg. However, the alternative scenario, in which dissociation proceeds through a late TS, is also plausible. If the acyl chain is extensively hydrated in the TS, such that there is no significant net change in vibrational frequencies along the reaction coordinate, no KIE would be detected. Indeed, the latter view of the dissociation mechanism is consistent with that drawn in the recent comparison of the E_a values for the dissociation of (Lg + FA) complexes in aqueous solution and the corresponding gaseous deprotonated (Lg + FA)^{*n*-} ions, where $n = 6$ and 7 , *vide supra*.¹³ This conclusion is also supported by the findings of Bojesen and Bojesen, who investigated the thermodynamics and kinetics of bovine serum

albumin (BSA) binding to long-chain FAs.⁵³ From their analysis of the entropies and activation entropies determined for the dissociation of the (BSA + FA) complexes in water, they concluded that the apolar chains of the FAs are similarly hydrated in the TS and in aqueous solution.

CONCLUSIONS

In summary, deuterium KIEs for the dissociation of a protein–ligand complex in the gas phase are reported for the first time. Partial or complete deuteration of the acyl chain of PA results in measurable inverse KIEs for the dissociation of gaseous, deprotonated (Lg + PA)^{*n*-} ions. The magnitude of the KIE is temperature dependent, and Arrhenius analysis of the rate constants reveals that deuteration results in a decrease in the dissociation E_a . It is proposed that deuterium KIEs arise, at least in part, from differential changes in the vibrational frequencies of the deuterated and non-deuterated complex, resulting from cleavage of the Lg–FA interactions, along the reaction coordinate. Furthermore, observation of a measurable KIE upon deuteration of only the methyl group of PA is consistent with the hypothesis of a late dissociative TS, wherein the acyl chain is close to being completely free of the binding pocket. In contrast, there is no measurable deuterium KIE for the dissociation of the (Lg + PA) complex in aqueous solution. It is proposed that the dissociation of the hydrated complex also proceeds through a late TS, in which the acyl chain is extensively solvated by water such that there is no significant change in vibrational frequencies along the reaction coordinate and, consequently, no KIE.

ASSOCIATED CONTENT

Supporting Information

Kinetic data for (Lg+PA)⁶⁻ ions, computed geometries, ZPEs, and internal energies. This information is available free of charge via the Internet at <http://pubs.acs.org>.

AUTHOR INFORMATION

Corresponding Author

john.klassen@ualberta.ca

Notes

The authors declare no competing financial interest.

ACKNOWLEDGMENTS

The authors are grateful for financial support provided by the Natural Sciences and Engineering Research Council of Canada and the Alberta Centre for Glycomics. A.B. thanks the Canadian Foundation for Innovation (New Opportunities Fund) for support for computational infrastructure. The computational work has been (partially) enabled by use of resources from Westgrid and Compute/Calcul Canada.

REFERENCES

- (1) Cleveland, D. W.; Mao, Y.; Sullivan, K. F. *Cell* **2003**, *112*, 407–421.
- (2) Helnius, A.; Aebi, M. *Science* **2001**, *23*, 2354–2369.
- (3) Igakura, T.; Stinchcombe, J. C.; Goon, P. K. C.; Taylor, G. P.; Weber, J. N.; Griffiths, G. M.; Tanaka, Y.; Osame, M.; Bangham, C. R. M. *Science* **2003**, *299*, 1713–1716.
- (4) Huang, J. F.; Yang, Y.; Sepulveda, H.; Shi, W. X.; Hwang, I.; Peterson, P. A.; Jackson, M. R.; Sprent, J.; Cai, Z. L. *Science* **1999**, *286*, 952–954.
- (5) Bizzarri, A. R.; Cannistraro, S. *J. Phys. Chem. B* **2009**, *113*, 16449–16464.

- (6) Chang, C. A.; Trylska, J.; Tozzini, V.; McCammon, J. A. *Chem. Biol. Drug. Des.* **2007**, *69*, 5–13.
- (7) Meltzer, R. H.; Thompson, E.; Soman, K. V.; Song, X.; Ebalunode, J. O.; Wensel, T. G.; Briggs, J. M.; Pedersen, S. E. *Biophys. J.* **2006**, *91*, 1302–1314.
- (8) Chilkoti, A.; Stayton, P. *J. Am. Chem. Soc.* **1995**, *117*, 10622–10628.
- (9) Schwesinger, F.; Ros, R.; Strunz, T.; Anselmetti, D.; Guntherodt, H.-J.; Honegger, A.; Jermutus, L.; Tiefenauer, L.; Pluckthun, A. *Proc. Natl. Acad. Sci. U.S.A.* **2000**, *97*, 9972–9977.
- (10) Long, D.; Mu, Y.; Yang, D. *PLoS ONE* **2009**, *4*, e6081.
- (11) Regan, C. K.; Craig, S. L.; Brauman, J. I. *Science* **2002**, *295*, 2245–2247.
- (12) Garver, J. M.; Fang, Y.; Eyet, N.; Villano, S. M.; Bierbaum, V. M.; Westaway, K. C. *J. Am. Chem. Soc.* **2010**, *132*, 3808–3814.
- (13) Liu, L.; Michelsen, K.; Kitova, E. N.; Schnier, P. D.; Klassen, J. S. *J. Am. Chem. Soc.* **2010**, *132*, 17658–17660.
- (14) Liu, L.; Bagal, D.; Kitova, E. N.; Schnier, P. D.; Klassen, J. S. *J. Am. Chem. Soc.* **2009**, *131*, 15980–15981.
- (15) Kontopidis, G.; Holt, C.; Sawyer, L. *J. Dairy Sci.* **2004**, *87*, 785–796.
- (16) Qin, B. Y.; Bewley, M. C.; Creamer, L. K.; Baker, H. M.; Baker, E. N.; Jameson, G. B. *Biochemistry* **1998**, *37*, 14014–14023.
- (17) Wade, D. *Chem.-Biol. Interact.* **1999**, *117*, 191–217.
- (18) Silva, R. G.; Rosado, L. A.; Santos, D. S.; Basso, L. A. *Arch. Biochem. Biophys.* **2008**, *471*, 1–10.
- (19) Loveridge, E. J.; Allemann, R. K. *Biochemistry* **2010**, *49*, 5390–5396.
- (20) Sucharitakul, J.; Wongnate, T.; Chaiyen, P. *Biochemistry* **2010**, *49*, 3753–3765.
- (21) Sen, A.; Kohan, A. *J. Phys. Org. Chem.* **2010**, *23*, 613–619.
- (22) Gawlita, E.; Caldwell, W. S.; O'Leary, M. H.; Paneth, P.; Anderson, V. E. *Biochemistry* **1995**, *34*, 2577–2583.
- (23) Fleming, D. G.; Arseneau, D. J.; Sukhorukov, O.; Brewer, J. H.; Mielke, S. L.; Schatz, G. C.; Garrett, B. C.; Peterson, K. A.; Truhlar, D. G. *Science* **2011**, *331*, 448–450.
- (24) Gola, A. A.; Sarzynski, D.; Drys, A.; Jodkowski, J. T. *Chem. Phys. Lett.* **2010**, *486*, 7–11.
- (25) Eyet, N.; Villano, S. M.; Kato, S.; Bierbaum, V. M. *J. Am. Soc. Mass Spectrom.* **2007**, *18*, 1046–1051.
- (26) Villano, S. M.; Kato, S.; Bierbaum, V. M. *J. Am. Chem. Soc.* **2006**, *128*, 736–737.
- (27) Schug, K. A.; Maier, N. M.; Lindner, W. *J. Mass Spectrom.* **2006**, *41*, 157–161.
- (28) Dunbar, R. C.; McMahan, T. B. *Science* **1998**, *279*, 194–197.
- (29) Price, W. D.; Schnier, P. D.; Jockusch, R. A.; Strittmatter, E. R.; Williams, E. R. *J. Am. Chem. Soc.* **1996**, *118*, 10640–10644.
- (30) Becke, A. D. *J. Chem. Phys.* **1993**, *98*, 5648–5652.
- (31) Becke, A. D. *Phys. Rev. A* **1988**, *38*, 3098–3100.
- (32) Lee, C.; Yang, W.; Parr, R. G. *Phys. Rev. B* **1988**, *37*, 785–789.
- (33) Vosko, S. H.; Wilk, L.; Nusair, M. *Can. J. Phys.* **1980**, *58*, 1200–1211.
- (34) Perdew, J. P.; Burke, K.; Ernzerhof, M. *Phys. Rev. Lett.* **1996**, *77*, 3865–3868.
- (35) Adamo, C.; Barone, V. *J. Chem. Phys.* **1999**, *110*, 6158–6169.
- (36) Ernzerhof, M.; Scuseria, G. E. *J. Chem. Phys.* **1999**, *110*, 5029–5036.
- (37) Hehre, W. J.; Radom, L.; Schleyer, P. v. R.; Pople, J. A. *Ab Initio Molecular Orbital Theory*; John Wiley and Sons: New York, 1985.
- (38) Scalmani, G.; Frisch, M. J. *J. Chem. Phys.* **2010**, *132*, 114110.
- (39) Cancès, E.; Mennucci, B.; Tomasi, J. *J. Chem. Phys.* **1997**, *107*, 3032–3041.
- (40) Cossi, M.; Scalmani, G.; Rega, N.; Barone, V. *J. Chem. Phys.* **2002**, *117*, 43–54.
- (41) Frisch, M. J.; Trucks, G. W.; Schlegel, H. B.; Scuseria, G. E.; Robb, M. A.; Cheeseman, J. R.; Scalmani, G.; Barone, V.; Mennucci, B.; Petersson, G. A.; Nakatsuji, H.; Caricato, M.; Li, X.; Hratchian, H. P.; Izmaylov, A. F.; Bloino, J.; Zheng, G.; Sonnenberg, J. L.; Hada, M.; Ehara, M.; Toyota, K.; Fukuda, R.; Hasegawa, J.; Ishida, M.; Nakajima, T.; Honda, Y.; Kitao, O.; Nakai, H.; Vreven, T.; Montgomery, Jr., J. A.; Peralta, J. E.; Ogliaro, F.; Bearpark, M.; Heyd, J. J.; Brothers, E.; Kudin, K. N.; Staroverov, V. N.; Kobayashi, R.; Normand, J.; Raghavachari, K.; Rendell, A.; Burant, J. C.; Iyengar, S. S.; Tomasi, J.; Cossi, M.; Rega, N.; Millam, N. J.; Klene, M.; Knox, J. E.; Cross, J. B.; Bakken, V.; Adamo, C.; Jaramillo, J.; Gomperts, R.; Stratmann, R. E.; Yazyev, O.; Austin, A. J.; Cammi, R.; Pomelli, C.; Ochterski, J. W.; Martin, R. L.; Morokuma, K.; Zakrzewski, V. G.; Voth, G. A.; Salvador, P.; Dannenberg, J. J.; Dapprich, S.; Daniels, A. D.; Farkas, Ö.; Foresman, J. B.; Ortiz, J. V.; Cioslowski, J.; Fox, D. J. *Gaussian 09*, Revision B.01; Gaussian, Inc.: Wallingford CT, 2009.
- (42) McClurg, R. B.; Flagan, R. C.; Goddard, W. A. III. *J. Chem. Phys.* **1997**, *106*, 6675–6680.
- (43) Ayala, P. Y.; Schlegel, H. B. *J. Chem. Phys.* **1998**, *108*, 2314–2325.
- (44) McClurg, R. B. *J. Chem. Phys.* **1996**, *111*, 7163.
- (45) Qvist, J.; Davidovic, M.; Hamelberg, D.; Halle, B. *Proc. Natl. Acad. Sci. U.S.A.* **2008**, *105*, 6296–6301.
- (46) Shi, B.; Davis, B. H. *J. Chromatogr. A* **1993**, *654*, 319–325.
- (47) Baweja, R. *Anal. Chim. Acta* **1987**, *192*, 345–348.
- (48) Turowski, M.; Yamakawa, N.; Meller, J.; Kimata, K.; Ikegami, T.; Hosoya, K.; Tanaka, N.; Thornton, E. R. *J. Am. Chem. Soc.* **2003**, *125*, 13836–13849.
- (49) Cameron, D. G.; Hsi, S. C.; Umemura, J.; Mantsch, H. H. *Can. J. Chem.* **1981**, *59*, 1357–1359.
- (50) Capelli, C.; Monti, S.; Scalmani, G.; Barone, V. *J. Chem. Theory Comput.* **2010**, *6*, 1660–1669.
- (51) Bouteiller, Y.; Pouilly, J.-C.; Grégoire, G. *Comput. Theor. Chem* **2011**, *966*, 220–224.
- (52) Merrick, J. P.; Moran, D.; Radom, L. *J. Phys. Chem. A* **2007**, *111*, 11683–11700.
- (53) Bojesen, E.; Bojesen, I. *J. Phys. Chem.* **1996**, *100*, 17981–17985.